

See discussions, stats, and author profiles for this publication at: <https://www.researchgate.net/publication/304019750>

Modelling of Photochemical Smog

Chapter · January 2002

DOI: 10.1007/978-3-662-04868-9_10

CITATION

1

READS

900

3 authors:



Hiep Duc

NSW Department of Climate Change, Energy, the Environment and Water

166 PUBLICATIONS 1,575 CITATIONS

[SEE PROFILE](#)



Vo Anh

University of Economics and Law

307 PUBLICATIONS 9,547 CITATIONS

[SEE PROFILE](#)



Merched Azzi

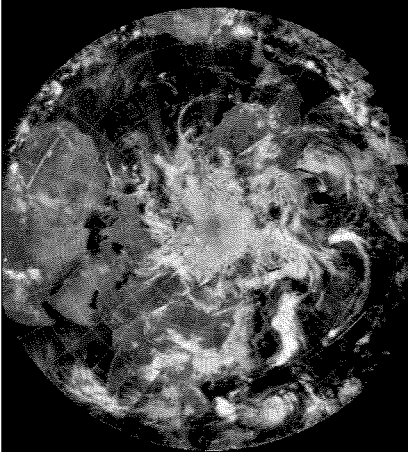
Office of Environment and Heritage

155 PUBLICATIONS 2,115 CITATIONS

[SEE PROFILE](#)

Gongbing Peng
Lance M. Leslie
Yaping Shao
Editors

Environmental Modelling and Prediction



10. Modelling of Photochemical Smog

Hiep Duc, Vo Anh and Merched Azzi

This chapter is concerned with air chemistry and its applications in air-quality modelling. Photochemical smog, i.e., the formation of high ground-level ozone concentrations, has been one of the main topics of air quality research in the last three decades. The chemistry of ground-level ozone is different from that of stratospheric ozone. Photochemical smog is a anthropogenic air pollution problem in many urban areas around the world, which is related to population increases and the reliance on motor vehicles for transport.

There are gaseous and particle pollutants, both of which have health effects. Many studies have been carried out on the effects of carbon monoxide, sulfur dioxides, nitrogen oxides, ozone and fine particles on mortality rates, respiratory and cardiac symptoms such as asthma, bronchitis and angina attacks. Apart from fine particles, smog formation during summer can produce high levels of ozone, hence degrading the air quality in the environment. The photochemistry of ozone formation is complex. In some urban airshed models there are hundred of equations involving many chemical species.

The mechanism of smog formation has been studied by the Commonwealth Scientific and Industrial Research Organisation of Australia (CSIRO) in smog chamber experiments. A simple semi-empirical model has been formulated to reduce the complexity of the photochemical reaction, which involves nitrogen oxides and reactive organic compounds under strong sunlight. This model is called the Integrated Empirical Rate (IER) model. In addition, a set of reaction equations has been proposed to simplify the explanation of the smog formation. This Generic Reaction Set (GRS) only involves seven reaction equations. In this chapter, we describe both the IER model and GRS mechanism and their application to air quality modelling.

10.1 Air Chemistry of Smog Formation

10.1.1 Chemistry of Ground Level Ozone Formation

Ozone is a reactive and unstable form of oxygen, often found at relatively high concentration during hot and hazy summer weather. Such haze may

build up over a period of days into a “photochemical smog”. The yellow or brownish colour of the smog is due to fine particles, rather than ozone which is invisible.

Unlike most other air pollutants, ozone is not directly emitted, but forms in air when strong sunlight acts on a mixture of hydrocarbons and nitrogen oxides (ozone precursors). High concentrations of ozone can irritate eyes and throat, cause headaches, bronchial irritation and shortness of breath, and produce an acrid taste and smell. Ozone also damages plants, weakens rubber and attacks metals and painted surfaces.

Ozone production in the troposphere requires the photolysis of nitrogen dioxide NO_2 , in turn, NO_2 is produced by reaction of NO with either ozone or peroxy radicals. Ozone can accumulate only when sufficient peroxy radicals are present. NO_x is removed from the NO-to- NO_2 -to-NO cycle by the reaction of NO_2 with radicals to produce stable gaseous nitrogen and stable non-gaseous nitrogen. Since radical reactions results in both ozone formation and conversion of NO_x to its reaction products, a correlation of ozone with NO_x should occur whether or not NO_x is the limiting precursor.

The chemistry of ozone in the atmosphere is highly complex and is difficult to simulate successfully with computer models, which are the main tools used to devise control strategies. This poses a ongoing challenge to air quality managers in their quest for the most efficient means to target pollution sources which contribute to ozone.

Ozone formation was extensively studied at the Division of Coal and Energy of the CSIRO using environmental chamber experiments. The smog chamber results enabled the rates of smog producing processes to be elucidated and provided the missing key for quantifying the atmospheric processes. This CSIRO innovation was called the Integrated Empirical Rate (IER) approach and the Generic Reaction Set (GRS) model.

By identifying the key property of reactive organic compounds (ROC) to be the photolytic rate coefficient for photochemical smog oxidant formation (R_{smog}), the quantitative description of photochemical smog was made tractable.

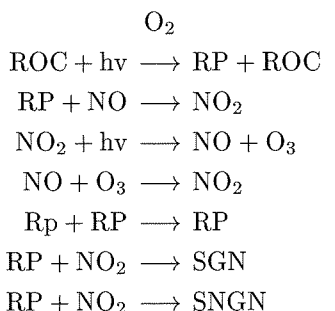
Ozone pollution is greatly influenced by weather conditions. A combination of light winds and strong sunshine, persisting with little change over several days, allows ozone precursor compounds to build up with little dilution. Under these conditions, ozone concentrations often rise progressively day by day as long as the warm, stable weather lasts. Because of the influence of weather, ozone pollution is highly variable from one year to the next. In warm summers, high ozone concentrations may be experienced repeatedly, whereas during more unsettled seasons, virtually no high values may be recorded.

10.1.2 Generic Reaction Set (GRS) Mechanism

The Generic Reaction Set (GRS) resulting from the smog chamber work is a type of photochemical reaction mechanism that utilises a set of only seven generic equations, but allows for the speciation of the individual reactive compound (ROC) precursors.

Traditionally the quantitative description of the chemical processes which give rise to photochemical smog has been approached via lengthy and detailed chemical mechanisms. These types of models require extensive computing resources and are difficult to implement and verify. In contrast, the GRS mechanism has the advantages of rapid computer execution and that, for the atmosphere, the principal rate coefficient can be measured in real time (by the Airtrak air monitoring system) thus providing a straightforward and practical means for the validation of airshed models which incorporate the GRS approach.

The GRS model consists of the following seven reactions

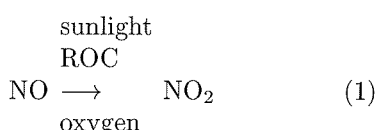


where: ROC = Reactive Organic Compound, RP = Radical Pool, SGN = Stable gaseous nitrogen products, and SNGN = stable non gaseous nitrogen products.

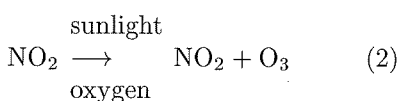
This can be compared with other mechanisms, such as Carbon Bond IV (CB-IV) mechanism containing 70 chemical reactions and 28 species or the California Institute of Technology (CIT) lumped molecule model containing 52 reactions and 32 species (Hess et al., 1992).

GRS mechanism has been applied in a number of studies (Venkatram et al., 1997; MAQSP, 1996). The GRS mechanism also have been included in the airshed modeling (MAQSP, 1996), in which a modified CIT airshed model with the LCC chemical mechanism was replaced by GRS mechanism. The results from the two model outputs are comparable.

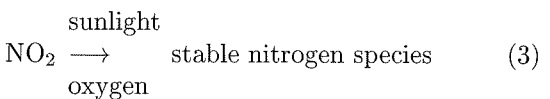
The Generic Reaction Set (GRS) model is based on the representation of all processes that lead to ozone formation. Firstly, the chemical mechanism of NO_2 and O_3 production is started. The sunlight induces photochemical reactions in the ROC species, producing strongly oxidising peroxy species and these oxidise NO to NO_2 ,



Then NO_2 can itself be photolysed, producing O_3 and regenerating NO



The NO regenerated is then free to again participate in another oxidation cycle. This process can continue producing ozone until there is insufficient NO available to sustain reaction (1). This occurs when competing reactions consume the nitrogen oxides and produce stable products such as nitric acid and nitrogenous aerosol particles,



A further complication which needs to be considered is the reaction of NO with O_3 , which is rapid and produces NO_2 ,



Thus there are two means by which NO can be oxidised to NO_2 , namely by reactions (1) and (4). When NO is emitted into air which already contains ozone, reaction (4) is important and NO immediately reacts with O_3 to form NO_2 until either the NO or O_3 is consumed. On the other hand, if the air has little O_3 content, the rate of NO_2 production will be governed by the rate of reaction (1), that is by the concentration of ROC and the intensity of sunlight. The rate of reaction (1) is also temperature sensitive, the rate increasing with increasing temperature. Thus the same factors (i.e. sunlight intensity, ROC concentration and temperature) dictate the production in the air of both NO_2 and O_3 [via reactions (1) and (2)].

10.1.3 Integrated Empirical Rate (EIR) Model

Photochemical smog formation is a complex process. To reduce the complexities and still have the ability to access fairly accurately and interpret air quality data, a semi-empirical model, resulted from smog chamber studies, has been formulated. This model is called Integrated Empirical Rate (IER) model. The method is based on quantifying photochemical smog in terms of NO oxidation.

The IER model defines Smog Produced (SP) as the quantity of NO consumed by photochemical processes plus the quantity of O_3 produced. A key

feature of the IER model is that SP increases approximately linearly with respect to cumulative sunlight exposure during a light-limited regime, until the available NO_x are consumed by reaction, then the NO_x -limited regime occurs and SP production ceases.

The current concentration of SP compared to the SP concentration that would be present if the NO_x -limited regime existed is indicative of how far toward attaining the NO_x -limited regime the photochemical reactions have progressed. During the light-limited regime, SP is calculated from the expression

$$SP(t) = R_{\text{smog}}(t) \int J_{\text{NO}_2} f(T(t)) dt \quad (10.1)$$

where R_{smog} is the photolytic rate coefficient (measured directly from the CSIRO Airtrak system), J_{NO_2} is the rate coefficient for NO_2 photolysis (a measure of sunlight intensity), $f(T)$ is a function of temperature.

$$f(T) = \exp \left[-1000\gamma \left(\frac{1}{T} - \frac{1}{360} \right) \right] \quad (10.2)$$

$\gamma = 4.7$ from the smog chamber studies, T is given in $^{\circ}\text{K}$.

For the NO_x -limited regime, where there is no new smog production, the concentration of SP is at its maximum and is proportional to the NO_x previously emitted in the air

$$SP_{\text{max}}(t) = \beta \text{NO}_x^0(t) \quad (10.3)$$

$\beta = 4.1$ from the smog chamber studies.

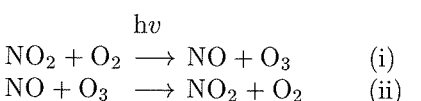
The ratio $E(t) = \frac{SP(t)}{SP_{\text{max}}}$ is then defined as the extent of smog produced.

When $E = 1$, smog formation is in the NO_x -limited regime and the NO , NO_2 concentration approach zero. When $E < 1$, smog production is in the light-limited regime.

Model description. The IER model defines the formation of photochemical oxidants in terms of "Smog Produced" (SP) where SP represents the concentration of NO consumed by photochemical processes plus the concentration of O_3 produced, viz.,

$$[SP]_0^t = [\text{NO}]_0^t - [\text{NO}]^t + [\text{O}_3]^t - [\text{O}_3]_0^t \quad (10.4)$$

where $[\text{NO}]_0^t$ and $[\text{O}_3]_0^t$ denote the NO and O_3 concentrations that would exist in the absence of atmospheric chemical reactions occurring after time $t = 0$ and $[\text{NO}]^t$ and $[\text{O}_3]^t$ are the NO and O_3 concentrations existing at time t . $[SP]_0^t$ denotes the concentration of smog produced by chemical reactions occurring during time $t = 0$ to time $t = t$. The use of the parameter SP to describe smog production removes the complicating influences of the following competing chemical reactions (i) and (ii):



The IER model provides an alternative concept of smog description by treating smog production as a function of the cumulative exposure of the reactants to sunlight rather than as a function of time. From this representation it was shown there are two regimes for photochemical smog. Firstly smog produced increases approximately linearly with respect to the cumulative sunlight. This stage is called "light-limited regime". This is followed by the NO_x -limited regime where the concentrations of NO and NO_2 decrease to zero. During the NO_x -limited regime there is no new smog production and the concentration of SP was found to be proportional to the concentration of NO_x previously emitted into the air

$$[\text{SP}]_{\max} = \beta[\text{NO}_x]_0^t \quad (10.5)$$

where, from smog chamber data, the β coefficient for urban air can be assigned the value of 4.1. In this regime we can derive an expression for the ozone concentration as follows:

$$[\text{O}_3]^t = (\beta - F)[\text{NO}_x]_0^t \quad (10.6)$$

where the coefficient F is the proportion of NO_x emitted into the air in the form of NO; usually $F \approx 0.9$.

For the light-limited regime the concentration of smog produced, SP, at a given time t , can be written as:

$$[\text{SP}]^t = \int_0^t R_{\text{smog}}^t J_{\text{NO}_2}^t F(T^t) dt \quad (10.7)$$

where R_{smog} is the photolytic rate coefficient for smog production and J_{NO_2} is the rate coefficient for photolysis of NO_2 , a measure of sunlight intensity. $F(T)$ is the temperature function:

$$F(T) = \exp[-1000\gamma(1/T - 1/316)] \quad (10.8)$$

where γ is a temperature coefficient determined from smog chamber studies and has the value 4.7; T is given in °K.

The ratio of the current concentration of SP to the concentration that would be present if the NO_x -limited regime existed is defined as the parameter "Extent" of smog production (E) and is given by:

$$E^t = [\text{SP}]^t / [\text{SP}]_{\max} \quad (10.9)$$

When $E = 1$, smog production is in the NO_x -limited regime and the NO_2 concentration approaches zero. When $E < 1$, smog production is in the light-limited regime.

The IER approach also enables SP and $[\text{NO}_x]_0^t$ to be determined from ambient measurements of ozone and nitrogen oxides. For the light-limited regime, the smog production can be calculated as:

$$[\text{SP}]^t = ([\text{O}_3]^t + [\text{NO}_y]^t - [\text{NO}]^t - (1 - F)[\text{NO}_y]^t) / (1 - FP) \quad (10.10)$$

where $[\text{NO}_y]^t$ is the concentration of oxidised nitrogen conventionally measured by nitrogen oxides analysers and P is a coefficient for the loss of NO_x into species and forms not detected as NO_y . For urban air an appropriate value of P is 0.122.

For the NO_x -limited regime:

$$[\text{SP}]^t = \beta[\text{O}_3]^t / (\beta - F) \quad (10.11)$$

The value of $[\text{NO}_x]_0^t$ for ambient air can also be determined from monitoring data.

For the light-limited regime:

$$[\text{NO}_x]_0^t = ([\text{NO}_y]^t + P([\text{O}_3]^t - [\text{NO}]^t)) / (1 - FP) \quad (10.12)$$

and for the NO_x -limited regime:

$$[\text{NO}_x]_0^t = [\text{O}_3]^t / (\beta - F) \quad (10.13)$$

In addition to the nitrogen oxides and ozone concentration of the air it is also necessary to know the photolytic rate at which new smog will be produced [see (10.7)]. The key parameters, which determine this rate, are the sunlight intensity and the value of R_{smog} , a photolytic rate coefficient. The values of R_{smog} for ambient air are related to the emissions of ROC and R_{smog} values can be routinely measured with the Airtrak system, which was especially developed for this purpose (Blanchard et al., 1995). Airtrak also simultaneously determines the nitrogen oxides and ozone concentrations of the air.

Time series data from a monitoring station represents the concentrations of different air parcels as they reach the monitor. With suitably located monitoring stations use of such data removes the need to model or guess the composition of the ambient air with which the NO_x plume is expected to mix. This also has the advantage that the intrinsic variability in atmospheric composition can be taken into account.

The IER chemistry formulation shows that the chemical rate dependent processes are significant only to the light-limited regime and that during this regime the rate of SP production is independent of the atmospheric NO_x concentration. Thus, when the ambient air is in the light-limited regime, the SP formation is unchanged by the presence of additional NO_x from the chimney plume. During the NO_x -limited regime, mixing of additional NO_x from the plume into the surrounding air can cause resumption of SP formation. For NO_x -plumes these findings enable the IER-reactive plume model to be formulated so that the plume dispersion calculations can be carried out independently of the photochemical reaction modelling.

Application of the IER model has been used in a number of studies (Hess et al., 1992; Pryor, 1998; Blanchard et al., 1995). The simplicity of the IER numerical calculations and the ability to execute the model on the basis of air quality monitoring data are its most attractive uses. It gives a technique that is particularly useful for environmental impact assessments of NO_x sources that have moderate emissions rates and for experiments which can not support the cost of a full airshed study.

10.1.4 Application

An application of the IER model is to access the smog event at a particular day with Airtrak measurements. Observations were collected during three summer days (10–12 February, 1994) at Liverpool station on Sydney. These successive days cover three different categories of high, medium and low photochemical reactive air, respectively. Six minute averages of Airtrak data recorded during these three days are presented in Figs. 10.1a and b.

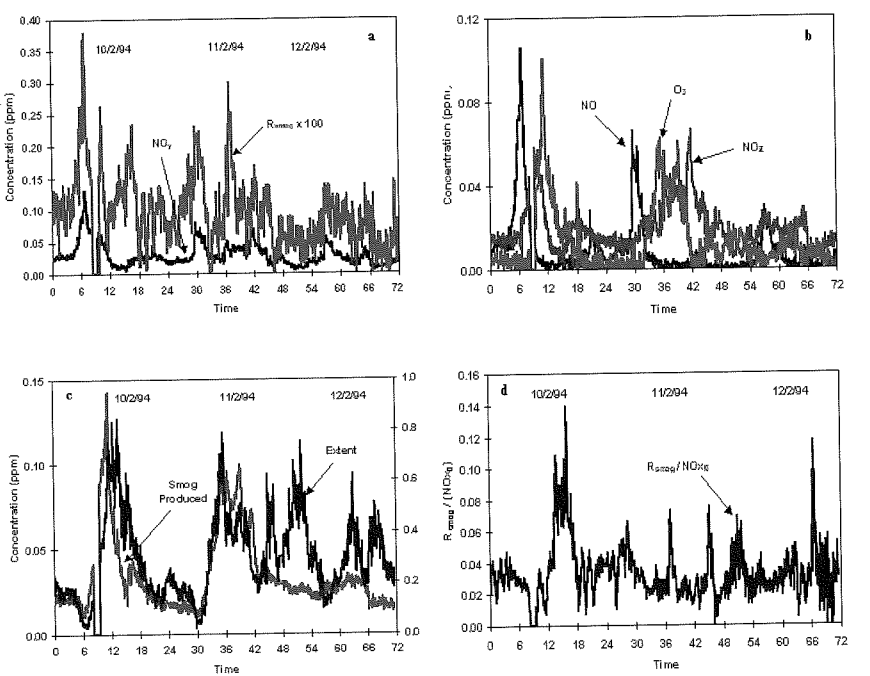


Fig. 10.1. (a) and (b) Airtrak measurements at Liverpool station in southwest of Sydney during February 10 to 12, 1994. (c) Calculated IER parameters using the model of Johnson and Azzi (1992). (d) the $(R_{\text{smog}}/\text{NO}_x)$ ratio.

The selected three days of Airtrak data were in good agreement with the simultaneous measurements taken by conventional instrumentation. On the 10th of Feb between 0830 hr and 0940 hr the Airtrak recorded data is missing. On the 10th of Feb between around 0940 hr and 1200 hr the ozone concentration is greater than 0.08 ppm. At other times the concentration is less than 0.06 ppm. On the 10th and 11th between 0500 hr and 0800 hr Fig. 10.1a indicates a plume of NO_x emissions and another plume of reactive organic compounds. On the 12th these plumes are not strongly pronounced.

The concentrations of NO, NO_y, O₃, and R_{smog} determined by Airtrak were used to calculate the various IER parameters according to version 2.2 of the model (Johnson and Azzi, 1992). The modeling results are given in Fig. 10.1c where the variation of smog production and extent are plotted in separate axis against time. As well, in Fig. 10.1d, the $(R_{\text{smog}}/\text{NO}_x)$ ratio is plotted against time showing how sensitive the photochemical smog formation is to changes in anthropogenic hydrocarbon and NO_x emissions. The IER modeling results show that the light-limited regime was dominating over the three days period where the extent parameter values were always less than 1 (Fig. 10.1d).

On the 10th, polluted air parcels were detected between 0930 hr and 1200 hr, and on the 11th polluted air parcels were detected between 1100 hr and 1500 hr. These parcels are characterised by a smog produced concentration greater than 0.8 ppm. In the morning before sunrise and after 2000 hr, the air sampled by Airtrak during the previous two days had the characteristics of clean or background air where SP and extent values were less than 0.02 ppm and 0.2 respectively. On the 12th the concentration of smog produced was less than 0.03 ppm all day indicating that there was no pollution episodes detected on this day.

Age of precursor emissions. The IER parameters, which describe the photochemical characteristic of an air parcel, can be used to approximate the parcel's age. The difference between the cumulative sunlight at the moment of sampling and the corresponding $\text{SP}/R_{\text{smog}}$ ratio, gives insight on how much the air parcel has been exposed to sunlight. The deduced value will allow a determination of the approximate time of precursor emissions.

A better estimation for the age of precursor emissions would be made by subtracting the existing background smog produced concentration allowing only the anthropogenic emissions to be evaluated. This can be done by using $(\text{SP} - \text{SP}_{\text{back}})/R_{\text{smog}}$ where SP_{back} is the time series of smog produced for background air. In the absence of any knowledge about the SP_{back} profile for the Sydney airshed and wishing to proceed with the selected Airtrak data analysis, we have adopted the following methodology: The following two values of SP_{back} 0.015 ppm and 0.030 ppm were used in this study. The modeling results, which are given in Fig. 10.2, show for every selected day four different plots designated by A, B, C, and D. The first, second and third were obtained by using $\text{SP}/R_{\text{smog}}$, $(\text{SP} - 0.015)/R_{\text{smog}}$, and $(\text{SP} - 0.03)/R_{\text{smog}}$ respectively.

and the fourth plot represents the cumulative sunlight profile for the selected day and its previous day.

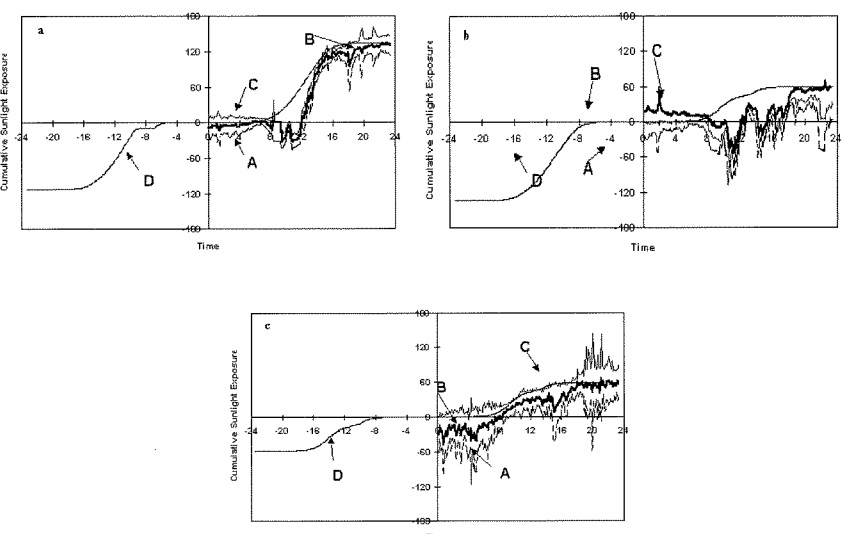


Fig. 10.2. Age of precursor emissions. (a) 10 February, 1994; (b) 11 February, 1994; (c) 12 February, 1994.

The ordinate serves to indicate how much cumulative sunlight an air parcel has seen. The time increments are quantified on the abscissa, which indicate how much time has elapsed before or after midnight of the selected day. The negative values indicate that the air parcel has been emitted from the previous day. For example, let us consider the plot A at 11am parcel on the 10th, the calculations indicate that the average time of precursor emissions was some 11 hours before midnight e.g. around 13pm from the previous day. The plots A, B, and C indicate the sensitivity of the method to the accuracy of the SP_{back} concentration. Since plot A does not have any SP_{back} correction, predictions of the age of the selected air parcels will be overestimated.

For a given SP_{back}, if the calculated value at a given time is higher than the corresponding cumulative sunlight value, then the used SP_{back} is not appropriate for that time. This can be seen on the following cases: on the 10th and 12th, between midnight and around 730 hr and between around 1800 hr and 2400 hr the use of plot C was not appropriate. On the 10th, the plot C was not appropriate between midnight and around 800 hr.

The relationships represented in Fig. 10.2 show that whatever the value used for SP_{back}, on the 10th, the air parcels sampled between around 930 hr and 1200 hr would be emitted in the afternoon of the previous day. On

the 11th and in the range of the variability of the selected SP_{back} the three plots show that the polluted episodes, ranged between 1000 hr and 1200 hr, originated from the previous day. On the 12th and in the accepted SP_{back} range of confidence, all plots can be fitted to have the shape of the corresponding cumulative sunlight profile without showing any time delay. The findings allow us to say that the 12th was a clean day.

The last two days illustrate that the air parcels passing the Airtrak have a low extent, indicating that they have either not received sufficient light flux to generate substantial photochemical products, or the dispersion of pollutants was high. These assumptions can be verified if we refer to an available windfield for these selected days.

The data sets from three selected Airtrak in the Liverpool area were implemented in the IER model to assess the air quality of the area. These Airtrak data sets show typical levels for NO, NO_y, NO₂, O₃ and R_{smog}. Airtrak measurements were in general agreement with measurements taken with conventional instruments. The IER parameters have produced information about ambient air quality including the age of the photochemical episodes precursors. This analysis provides valuable and effective tools for assessing ozone precursor control strategies. In addition, the Airtrak data analysis has shown that it is necessary to predict the background SP concentration to allow higher accuracy for an effective control strategy to take place.

10.2 Air Chemistry in Air Quality Modelling

10.2.1 Review of Air Quality Modelling

There are a significant number of air quality models, which have been used, applied and described in the literature. The models range from simple to large and highly complex mathematical modelling of the physical phenomena. The different kind of models can also be classified as empirical/statistically-based or physically-based models. In general, physically-based models are too large and complex to be used on a personal computer to predict and forecast the behaviour of the physical system under consideration.

The progress of air quality modelling is associated with the advance in the computing technology. In the past 3 decades, air quality models have been developed from simple box models and Gaussian models in the early 1970s to the advanced Eulerian and Lagrangian models currently used. Reviews of these models can be found in Collett and Odumemi (1997) and Zanetti (1990).

Eulerian models use a stationary frame of reference, in which the concentration field relative to the domain is derived. In these models, the equation for the mass conservation of a species *c* is

$$\frac{\partial c_i}{\partial t} = -\bar{U} \cdot \nabla c_i - \nabla \cdot c'_i U' + D \nabla^2 c_i + S_i \quad (10.14)$$

where the wind field vector $U = \bar{U} + U'$ and the concentration of species i , $c_i = \bar{c}_i + c'_i$ consist of an average component (\bar{U} or \bar{c}_i) and a fluctuating component (U' or c'_i).

The first 3 terms on the right hand side of the above equation represent the rate of advection by wind motion, rate of turbulent diffusion and rate of molecular diffusion of pollutant species. The last term represents the contribution from sources or sinks (e.g. deposition) of the species. In most cases, the rate of molecular diffusion can be neglected and the rate of turbulent diffusion in the second term can be assumed to follow a "first-order" equation in which the diffusion rate is linearly proportional to the local concentration. This method is also called the K theory of diffusion.

Lagrangian models use a reference system which follows the prevailing vector of atmospheric motion. The general atmospheric dispersion equation for a species is (Collett and Oduyemi, 1997)

$$c(\mathbf{r}, t) = \int_{-\infty}^t \int p(\mathbf{r}, t | \mathbf{r}', t') S(\mathbf{r}', t') d\mathbf{r}' dt' \quad (10.15)$$

where $c(\mathbf{r}, t)$ is the average concentration of the species at location \mathbf{r} at time t , $S(\mathbf{r}', t')$ is the source term and $p(\mathbf{r}, t | \mathbf{r}', t')$ is the probability density function that an air parcel is moving from \mathbf{r}' at time t' to \mathbf{r} at time t .

The Lagrangian model requires more intensive computing resources compared to the Eulerian model. One of the difficulties with Lagrangian models is that their results can not be easily compared with observed measurements (Collett and Oduyemi, 1997).

The newest breed of models are the Lagrangian particle models. These models combine both Eulerian and Lagrangian approaches in which the conceptual view of "inert particles" being transported through a domain as a result of force applying on them. Various methods have been used and applied in the majority of current models using this approach.

These atmospheric dispersion models are strongly influenced by meteorological conditions. Due to the lack (or the impracticality) of meteorological observations in the modelled domain, many models (especially the later advanced models) incorporate a full meteorological modelling component.

Many air quality and dispersion models are developed to estimate the near-field impacts from a variety of industrial point sources and are used for regulatory purposes in local and national environment agencies. In the USA, regulatory models such as the Industrial Source Complex Short-Term (ISCST2) (and its recently updated AERMOD model), Buoyant Line and Point Source (BLP), RAM, COMPLEX I, MESOPUFF, Rough Terrain Dispersion Model (RTDM), Shoreline Dispersion Model (SDM) are used by the US EPA and local environment authorities. Some of these models have been adapted and used in Australia.

These models mostly use the classic Gaussian dispersion method and involve a limited number of non-reactive pollutant species from industrial point

sources. Such models are usually less complex than those models used for research and planning of air quality control strategies in large urban domains, which have many point sources and a variety of diffuse sources. Large complex photochemical smog models are used for modelling air pollution events or simulations of different control scenarios in an urban airshed. These models contain many reactive species. Examples of such models are the Urban Airshed Model (UAM) developed by the US EPA or the one developed by the California Institute of Technology (CIT) for a large urban area such as the Los Angeles airshed.

In Europe, long distance photochemical smog models such as the EUMAC model used in EUROTRAC project or various models used in different countries (such as LOTOS in the Netherlands, PHOXA in Germany) are used to study the effects of Volatile Organic Compound (VOC) and NO_x control at regional (European) scale on ozone levels in Europe (Fowler et al., 1999).

Depending on the domain under consideration and its grid size, air quality models can also be classified into regional or long distance (global) transport models. Long distance transport models involve inter-regional transport of air pollutants. Examples of such models are the EMEP model used for SO₂ or ozone transport across Europe or the Regional Acidic Deposition Model (RADM) used in the USA for modelling SO₂ deposition across the Eastern USA.

Air quality models are also designed for modelling different pollutants: gaseous pollutants (such as sulfur dioxide, ozone or photochemical smog) and particles. The most complex of these is the photochemical smog model. As the species are reactive, the air chemistry component in the model, reflecting the complex mechanism of ozone formation in the atmosphere under sunlight with many air pollutants, is substantial.

10.2.2 Air Pollution Forecasting Using GRS and Reactive State-space Models

There is a need for a simple system to predict and forecast the level of ozone in an operational network of monitoring stations in an urban area. Many of the existing operational forecasting schemes, used by many environment authorities, are based on the knowledge of meteorological conditions. The GRS model is implemented in the multivariate model of three main species of ozone, nitrogen oxide and nitrogen dioxides in the form of state-space equations. Because of the nature of reaction between the three variables, this model is called the reactive state-space model.

The model is developed and reduced to a Kalman filtering system suitable for implementation in a fast algorithm on the computer. The advantage of this model is that it is simple, accurate and fast enough to be used on an operational daily basis. In contrast, the mechanism for photochemical smog formation as used in the airshed models (such as the Carbon Bond IV (CB-IV) with 78 reactants and 170 reactions (Gerry et al., 1988; Morris et

al., 1990) as used in the US EPA Urban Airshed Model (UAM), or in the California Institute of Technology (CIT) Model is too complex and CPU intensive to be used routinely.

10.2.3 The Extended Space-time Model

The concentrations $c_i(x, y, z, t)$, $i = 1, \dots, n$ of n chemically reactive species are assumed to satisfy the mass conservation equations:

$$\frac{\partial c_i}{\partial t} + Lc_i = r_i + s_i + d_i = f_i \quad (10.16)$$

where r_i is the rate of formation of species i by chemical reaction, s_i is the rate of formation of species i from the sources and d_i is the rate of deposition of species i .

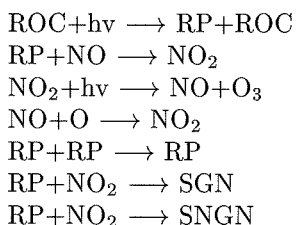
Under the assumptions of the K theory, the operator L takes the form

$$Lc_i = \bar{u}\frac{\partial c_i}{\partial x} + \bar{v}\frac{\partial c_i}{\partial y} + \bar{w}\frac{\partial c_i}{\partial z} - K_H \frac{\partial^2 c_i}{\partial x^2} - K_H \frac{\partial^2 c_i}{\partial y^2} - \frac{\partial}{\partial z} \left(K_V \frac{\partial c_i}{\partial z} \right) \quad (10.17)$$

where K_H and K_V are horizontal and vertical diffusivity constants and $\bar{u}, \bar{v}, \bar{w}$ are the deterministic wind velocity components in the x, y and z direction respectively.

10.2.4 The GRS Mechanism

The chemistry component of f_i of the above equation is based on the GRS mechanism, which consists of the following reactions:



where ROC = reactive organic compound (NMHC and oxygenated products); RP = radical pool (lumped radical species); SGN = stable gaseous nitrogen product; SNGN = stable non-gaseous nitrogen product.

Writing $[\text{O}_3](t)$ to mean the concentration of O_3 at time t , etc., the reaction rates for the above seven equations are given by

$$\begin{aligned} R_1 &= k_1[\text{ROC}] \\ R_2 &= k_2[\text{RP}] [\text{NO}] \\ R_3 &= k_3[\text{NO}_2] \end{aligned}$$

$$\begin{aligned} R_4 &= k_4[\text{NO}] [\text{O}_3] \\ R_5 &= k_5[\text{RP}] [\text{RP}] \\ R_6 &= k_6[\text{RP}] [\text{NO}_2] \\ R_7 &= k_7[\text{RP}] [\text{NO}_2] \end{aligned}$$

with k_i as the reactive constant of each of the above seven chemical reactions.

The chemical species that we interest in are ozone (O_3), nitrogen oxide (NO) and nitrogen dioxides (NO_2). By putting $c_1 = [\text{O}_3]$, $c_2 = [\text{NO}]$, $c_3 = [\text{NO}_2]$, the extended space-time model which combines advection, diffusion and GRS is

$$\frac{\partial c_1}{\partial t} = Lc_1 + k_3c_3(t) - k_4c_2(t)c_1(t) \quad (10.18)$$

$$\frac{\partial c_2}{\partial t} = Lc_2 + k_3c_3(t) - k_4c_2(t)c_1(t) - k_2[\text{RP}](t)c_2(t) + s_2 + d_2 \quad (10.19)$$

$$\begin{aligned} \frac{\partial c_3}{\partial t} = Lc_3 + k_2[\text{RP}](t)c_2(t) + k_4c_2(t)c_1(t) - k_3c_3(t) - \\ - k_6[\text{RP}](t)c_3(t) - k_7[\text{RP}](t)c_3(t) + s_3 + d_3 \end{aligned} \quad (10.20)$$

with boundary conditions $K_H = \frac{\partial c_i}{\partial z} = 0$, for $z = 0$ and $H(x, y, t) = 0$, $i = 1, 2, 3$, where $H(x, y, t)$ is the height of the inversion layer for the airshed under consideration.

In the above system, the next value of $[\text{RP}](t)$ is obtained from the current values of $[\text{O}_3]$, $[\text{NO}]$ and $[\text{NO}_2]$. Hence, the system must be solved recursively.

10.2.5 The State-space Form

For a discrete approximation to the above continuous system, we may consider forward time difference to approximate time derivatives, second-order centred finite difference to integrate the advection and horizontal diffusion terms as well as the Crank-Nicholson method to integrate the vertical diffusion term. The resulting system can then be written in the state-space form (Anh et al., 1998)

$$\begin{cases} c(t+1) = Ac(t) + B + \varepsilon(t) \\ y(t) = Hc(t) + u(t) \end{cases} \quad (10.21)$$

where $y(t)$ is the vector of concentrations observed at the sites, H is a matrix whose elements are either 0 or 1, the value 1 corresponding to a grid point coinciding with a site. The matrix A is determined by the diffusion and advection characteristics (diffusion constants and wind data). The matrix B contains by the chemistry and emission or deposition characteristics.

The covariance matrix $Q(t)$ of the state equation is taken to have the form

$$Q_{ij}(t) = E(\varepsilon_i(t)\varepsilon_j(t)) = \frac{r_{ij}}{2\alpha} K_1(\alpha r_{ij}) \quad (10.22)$$

where r_{ij} is the distance between site i and site j on the grid, and K_1 is the modified Bessel function of the second kind, order 1. The above form is deduced from the atmospheric diffusion equation of the K theory (Anh et al., 1997). Nonlinear least squares fitting to the cumulative semivariogram of monthly averaged ozone data at 18 monitoring stations of the Sydney region yields that $\alpha = 0.148$ for the period under study (January 1994). This form seems adequate in representing the spatial variability of a homogeneous and isotropic concentration field (Anh et al., 1997).

The elements of the covariance matrix $R(t)$ of the observation equation are set at the values

$$R_{ij}(t) = \begin{cases} 0.1 & i = j \\ 0 & i \neq j \end{cases}$$

to reflect moderate random errors in the measurements.

The system is derived for a species c_i . The complete system for c_1 , c_2 and c_3 can now be written in the state-space form above with

$$c = [c_1 \ c_2 \ c_3], \quad B = [B_1 \ B_2 \ B_3]^T, \quad \varepsilon = [\varepsilon_1 \ \varepsilon_2 \ \varepsilon_3]^T, \quad u = [u_1 \ u_2 \ u_3]^T$$

$$A = \begin{bmatrix} A_1 & 0 & 0 \\ 0 & A_2 & 0 \\ 0 & 0 & A_3 \end{bmatrix} \quad H = \begin{bmatrix} H_1 & 0 & 0 \\ 0 & H_2 & 0 \\ 0 & 0 & H_3 \end{bmatrix}$$

T denoting the transpose matrix. Since there is no change in the notation, we shall continue to use (10.21) to denote this complete system.

The Kalman algorithm for filtering and prediction of system (10.21) is

$$\begin{aligned} c(t|t) &= c(t|t-1) + G(t)(y(t) - Hc(t|t-1)) \\ c(t+1|t) &= Ac(t|t) + B \\ G(t) &= P(t|t-1)H'(HP(t|t-1)H' + R(t))^{-1} \\ P(t|t) &= (I - G(t)H)P(t|t-1) \\ P(t+1|t) &= AP(t|t)A' + Q(t+1) \end{aligned}$$

where $c(t|t)$ is the estimation of $c(t)$ based on the new data $y(t)$, $c(t+1|t)$ is the prediction of $c(t+1)$ made at time t , $G(t)$ is the Kalman gain, which gives a correction to the previous forecast $c(t|t-1)$, and $P(t|t-1)$ is the covariance matrix of the prediction error, which is recursively computed through the last two equations of the algorithm.

The system (10.21) for the three species c_1 , c_2 and c_3 is much more complex than those considered in Bankoff and Hanzevack (1975), Fronza et al. (1979) and Hernandez et al. (1991).

In these latter studies, the state-space form was obtained for a single species, while our system (10.21) allows for reactive relationships between the three species. These relationships connect and describe the reactive dynamics of the individual equations of the system. The Kalman algorithm also offers a convenient framework for determining the influence of different effects on the generation of c_1 , c_2 and c_3 . For example, under suitable conditions such as a calm day with strong sunlight, the chemistry component [mainly the matrix B in (10.21)] will be dominant in the algorithm. On the other hand, under different meteorological conditions such as strong wind, advective and diffusive transport will take effect while the chemical reaction rates become close to zero rendering the term B insignificant in the algorithm (apart from some adjustments for emissions and deposition rates).

10.2.6 Application

The state-space model, which accommodates the GRS photochemical mechanism, advection, diffusion and emissions, is applied to an irregular grid of monitoring network stations in Sydney, Australia. The location of these stations in the Sydney network (of 18 monitoring stations) is given in Fig. 10.3.

Two configurations of the Sydney monitoring network are considered:

- Grid A consisting of six stations: St Marys, Blacktown, Westmead, Lidcombe, Liverpool and Bringelly;
- Grid B consisting of seven stations: St Marys, Blacktown, Westmead, Lidcombe, Liverpool, Bringelly and Campbelltown.

The domain under consideration is urban. Two levels, namely the ground and the mixing height (maximum 2000 m above ground level) are considered since there are no observations currently available at the intermediate levels. Hence Grid A is considered as a rectangular grid with $L = 3$, $M = 2$, $N = 2$. January 9th 1994 is characterised by moderate concentrations of ozone in south west Sydney and is used as a test case. The data set consists of ten-minute observed concentrations of ozone, NO, NO₂, wind speed, wind direction, temperature, humidity and solar radiation at the monitoring stations. As an example, the time series of ozone concentrations for the six sites of Grid A are displayed in Fig. 10.4.

The diffusivity coefficients are obtained from the CSIRO Lagrangian atmospheric dispersion model (LADM), which is an air pollution dispersion model simulating the transport and diffusion of emissions of pollutants from discrete sources. It has a prognostic windfield component and a Lagrangian particle dispersion component (Physick et al., 1994).

The mixing height h is estimated using the diagnostic equations. For the period under study, neutral and stable conditions prevailed at night according to the wind speed classification, while unstable conditions are observed during the day.

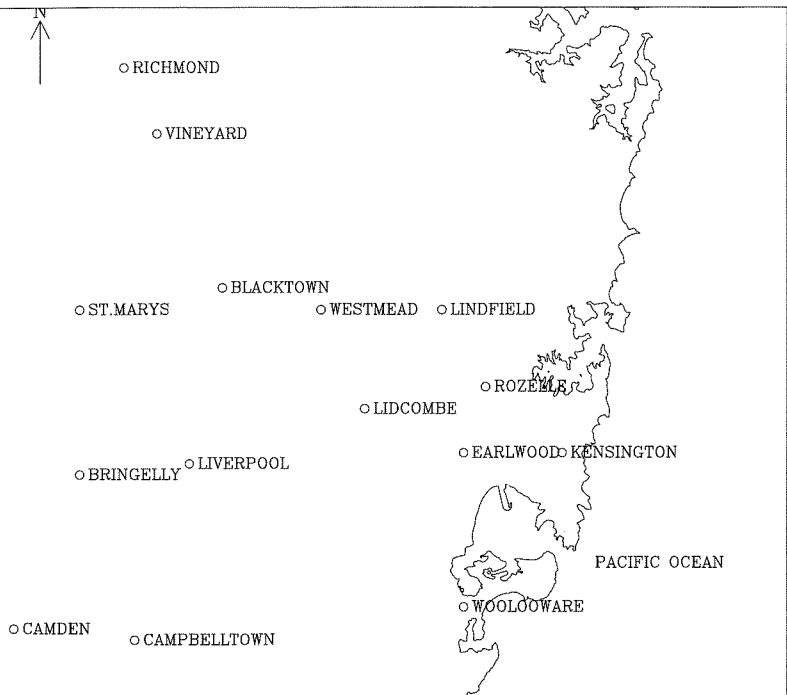


Fig. 10.3. Air quality monitoring stations in Sydney.

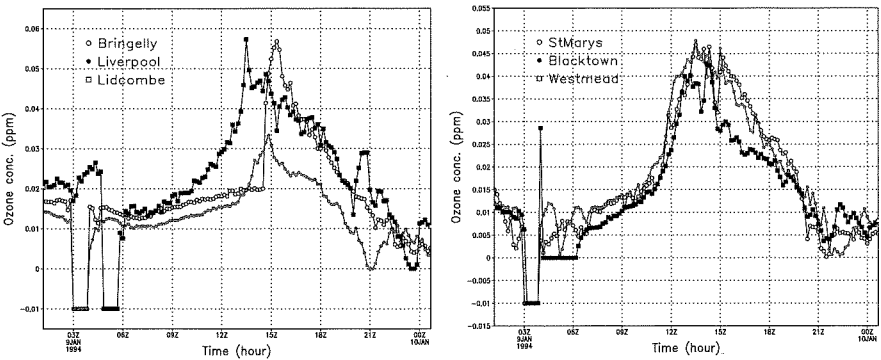


Fig. 10.4. Time series of ozone concentrations for the 6 sites.

The rate coefficients, as well as the observed values of a number of ROC mixtures, are obtained using the data from the CSIRO smog chamber experiments. These values are assumed for ambient Sydney suburban hydrocarbons. This is considered to be space and time-invariant and is consistent with the information on ROC from the existing NSW EPA emission inventory.

Due to lack of reliable data on emission and deposition rates, we follow Fronza et al. (1979), Melli et al. (1981) by heuristically correcting these values through an a posteriori pollutant mass balance, which is calculated from a comparison between filtered and previously predicted overall mass of pollutants at ground level. The filtering and prediction of O_3 , NO , NO_2 and RP are carried out in an iterative scheme. The algorithm is applied to Grid A, and one-step ahead forecasts are derived for O_3 , NO , NO_2 at each station.

As an example, the predicted and observed values of O_3 , NO and NO_2 are presented in Fig. 10.5 for Blacktown, and in Fig. 10.6 for Liverpool. Calibration was performed between 3 and 4 am, hence data was not available in this period and was set at -0.01. Due to this artificial setting, the Kalman filter would not trace out these values.

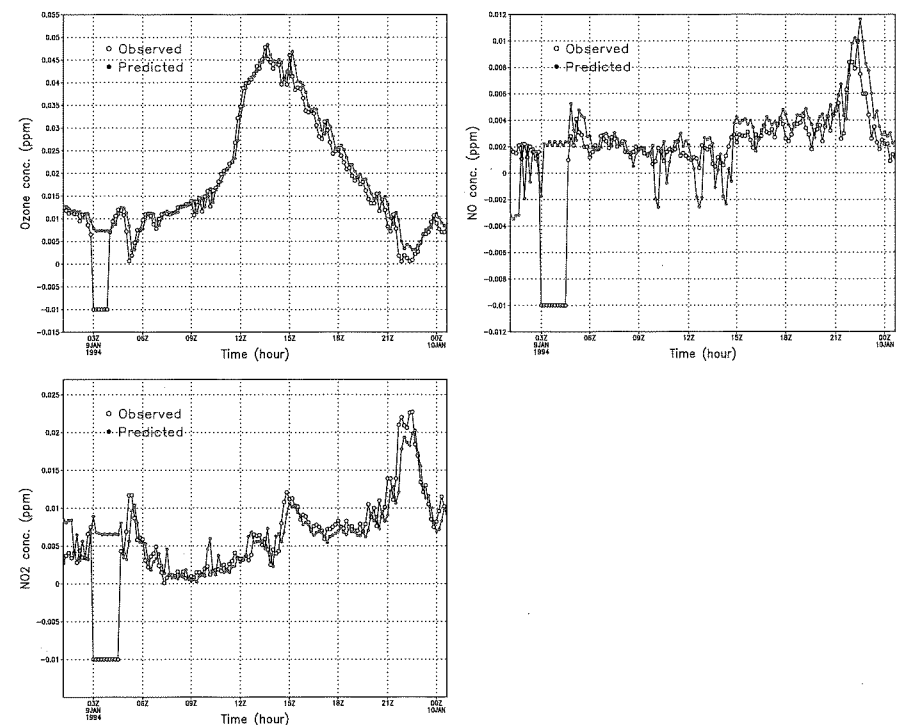


Fig. 10.5. Predicted and observed values of O_3 , NO and NO_2 for Blacktown.

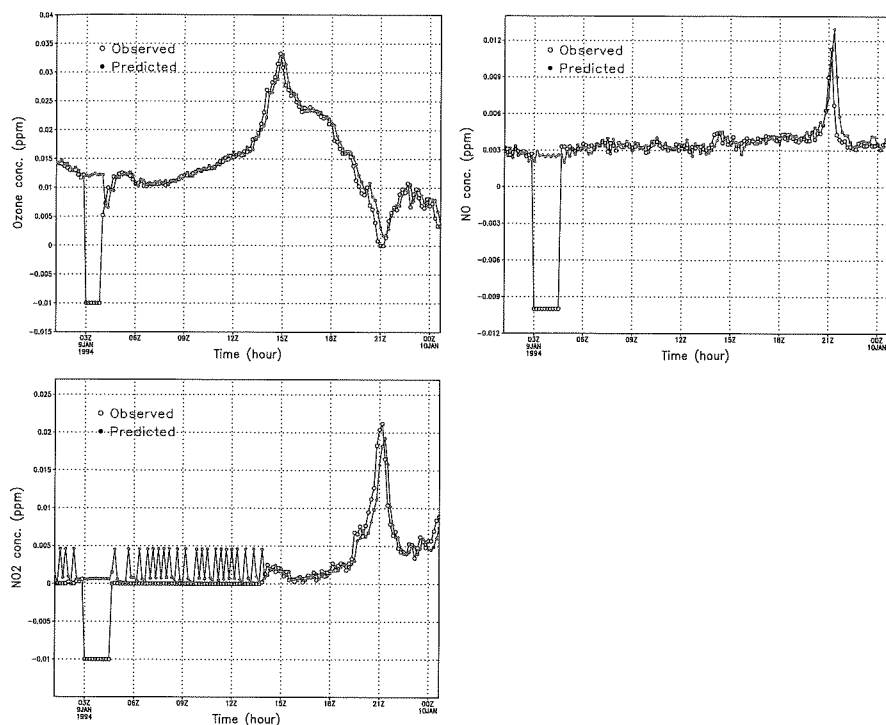


Fig. 10.6. Predicted and observed values of O_3 , NO and NO_2 for Liverpool.

The exercise is repeated for Grid B, where Campbelltown is added to Grid A; but in this exercise, we assumed that there were no measurements at Campbelltown. The Kalman filter is then activated based on information at the other six sites of the grid and produces one-step ahead forecasts for Campbelltown. The forecasts for ozone at Campbelltown are displayed in Fig. 10.7. The forecasts for NO and NO_2 at Campbelltown were also obtained; but since there are no observed values for them at this station, the results are not displayed here.

From Figs. 10.5 – 10.7, it is seen that the model works quite well, tracing out the pollution episodes closely in each case.

The space-time model which accommodates the main elements of air chemistry, advection, diffusion and emissions is put into the state-space form using appropriate stable numerical schemes which allow for irregular grids, a common feature of monitoring networks. The covariance structure of the noise term of the state equation reflects the spatial variability of the Sydney airshed established in a previous study.

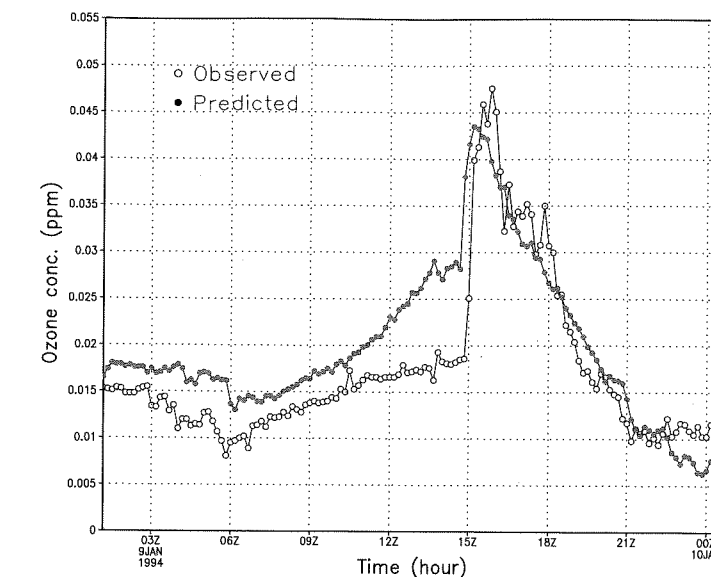


Fig. 10.7. Ozone forecast for Campbelltown.

Another significant contribution of this model is the modelling of the reactive dynamics of three key species (O_3 , NO, NO_2) of photochemical smog within a stochastic state-space framework. It should be noted that previous state-space models concentrated on a single species or several non-reactive species, hence were not concerned with reactive relationships between the species, which is an important aspect of photochemical smog production.

Due to its reasonably compact size and the fast Kalman algorithm, the model offers a tool for experimentation and scenario analyses, particularly suited to investigating the effect of different meteorological conditions on the generation of O_3 , NO, NO_2 . Numerical results on a grid of seven stations indicate that the performance of the model is quite credible in terms of producing forecasts for an unobserved location, which is a difficult but important task of airshed modelling.

The photochemical smog formation is represented by the GRS mechanism. Since the solution of the gas phase chemistry is typically the largest consumer of CPU time in air quality models, a simplified chemical reaction set, such as the GRS mechanism, is highly desirable. However, the mechanism lacks representation of inorganic processes, which may be important for the description of photochemical smog production in the NO_x -rich region, i.e. for low VOC-to- NO_x ratios of emissions.

In this case, it would be appropriate to use a more detailed model such as the condensed version of the non-linear Lurmann-Carter-Coyner (LCC) mechanism (Lurmann et al., 1987; Harley et al., 1993). This version includes 26 differential and 9 steady-state chemical species. In addition to eight lumped organic classes, the chemical mechanism explicitly includes the chemistry of methane, methanol, ethanol, methyl tert-butyl ether (MTBE), isoprene, hydrogen peroxide and sulfur dioxide. The chemistry of isoprene is relevant to the modelling of contributions of emissions from biogenic/natural sources to the urban photochemical smog development. This chemistry is used in the model as a surrogate for all biogenic hydrocarbon emissions. The oxygenated species (methanol, ethanol, and MTBE) are of interest because they are the main ingredients in alternative or reformulated fuels, which are introduced gradually in many states in the USA. However, MTBE is being withdrawn due to problems with the contamination of ground water.

11. Applications of Integrated Environmental Modelling

Yaping Shao and Sixiong Zhao

11.1 Recent Developments in Integrated Environmental Modelling

As mentioned in Chap. 2, environmental prediction involves the estimation of future environmental states for given current and/or past conditions. It consists of three categories, namely:

- The prediction of key variables that quantify the state of the individual components, such as wind, air temperature, humidity and precipitation for the atmosphere; flow speed, temperature and salinity for the ocean; or mass and area distribution of ice and snow, etc;
- The prediction of the exchange of mass, momentum and energy between the components, in association with major cycles in the environmental system, e.g., the cycles of water, energy, CO₂ and aerosol; and
- The prediction of environmental events and phenomena, such as severe weather, air- and water-pollution episodes, ozone concentration, dust storms, salinisation, etc.

From the time-scale perspective, environmental predictions can be divided into short-range (up to a few days), medium-range (several days to several weeks) and long-range predictions (weeks to decades). From the perspective of the spatial domain, they can be classified as local, regional or global.

The methods of environmental prediction include deterministic numerical modelling, statistical and dynamic-stochastic methods, or a combination of these (e.g., ensemble prediction). The choice of which method to use depends on the time scale of the problem concerned. Deterministic models are the most popular for environmental predictions at all temporal and spatial scales, although the general view is that they are most appropriate for short- to medium-range predictions. For medium- to long-range predictions, statistical and dynamic-stochastic methods are alternatives, as deterministic models become less reliable.

As the environment is inherently dominated by non-linear processes and interactions, there are no simple relations between its responses to external